



Thermal decomposition of a molecular material $\{N(n\text{-C}_4\text{H}_9)_4[\text{Fe}^{\text{II}}\text{Fe}^{\text{III}}(\text{C}_2\text{O}_4)_3]\}_{\infty}$ leading to ferrite: A reaction kinetics study

ASHIS BHATTACHARJEE^{1*}, DEBASIS ROY¹, MADHUSUDAN ROY²
and ARUNABHA ADHIKARI³

¹Department of Physics, Visva-Bharati University, Santiniketan, India, ²Applied Material Science Division, Saha Institute of Nuclear Physics, Kolkata, India and ³Department of Physics, West Bengal State University, Barasat, India

(Received 19 May 2012)

Abstract: A multi-step thermal decomposition of a molecular precursor, $\{N(n\text{-C}_4\text{H}_9)_4[\text{Fe}^{\text{II}}\text{Fe}^{\text{III}}(\text{C}_2\text{O}_4)_3]\}_{\infty}$ was studied using non-isothermal thermogravimetric (TG) measurements in the temperature range 300 to ≈ 800 K at multiple heating rates (5, 10 and 20 K min⁻¹). The thermal decomposition of the oxalate-based complex proceeded stepwise through a series of intermediate reactions. Two different isoconversional methods, namely, an improved iterative method and a model-free method were employed to evaluate the kinetic parameters: activation energy and rate of reaction. The most probable reaction mechanism of thermal decomposition was also determined. The different reaction pathways leading to different steps in the TG profile were also explored, which are supplemented by earlier experimental observations.

Keywords: molecular materials; oxalates; non-isothermal thermogravimetry; decomposition kinetics; model free methods.

INTRODUCTION

Among all nanomaterials, metal oxides are very attractive functional materials synthesized on the nanoscale. Their unique characteristics make them the most diverse class of materials with properties covering almost all aspects of solid-state physics and materials science. Metal oxides represent therefore essential constituents in technological applications such as magnetic storage,^{1,2} gas sensing^{3,4} and energy conversion,⁵ to name but a few. Various physical or chemical synthetic approaches for the synthesis of metal oxide nanoparticles have been developed over the years.⁶ Research was initiated aimed at the preparation of metal oxide nanoparticles using molecular metalorganic complexes as precur-

*Corresponding author. E-mail: ashis.bhattacharjee@visva-bharati.ac.in
doi: 10.2298/JSC120519145B

sors through the thermal decomposition route. The approach consisted of two steps: the synthesis of molecular metalorganic precursors in the first step and the oxidation of the precursor in a controllable manner in the second step. The precursors thermally degrade at different levels depending on the reaction conditions. It was conjectured that controlled oxidation through thermal decomposition of the precursors may lead to various metal oxide nanoparticles. Thus, by studying the solid-state thermal decomposition reaction kinetics of the precursors, the shape and size of the metal oxide nanoparticles could be monitored by externally controlling the different reaction kinetic parameters.

Polymeric bimetallic oxalate complexes of the general formula, $\{A[M^{II}M^{III}(C_2O_4)_3]\}_\infty$, (A: organic cation, M^{II} and M^{III}: di-/tri-valent transition metal ions; C₂O₄: oxalate ligand) have been important topics in the field of molecular magnetism.⁷ Thermal decomposition of a ferromagnetic material of this family, $\{N(n-C_4H_9)_4[Mn^{II}Cr^{III}(C_2O_4)_3]\}_\infty$ results in a spinel compound, Mn_{1.5}Cr_{1.5}O₄ at ≈ 500 °C.⁸ Recently, thermal decomposition of the molecular ferrimagnetic material $\{N(n-C_4H_9)_4[Fe^{II}Fe^{III}(C_2O_4)_3]\}_\infty$ was reported.^{9,10} It was seen that thermal decomposition leads to the formation of nano-sized ferrites. These results suggested that $\{A[M^{II}M^{III}(C_2O_4)_3]\}_\infty$ type molecular materials may be suitable single-molecular precursors for the synthesis of metal oxides *via* the thermal decomposition route. Moreover, the synthesis of these molecular materials is quite easy and economic, and the desired metal oxides could be prepared from such homo/heterometallic complexes at relatively low temperatures.

In light of the above, it was thought worthy to undertake a systematic study of the kinetics of the solid state thermal decomposition reaction of $\{N(n-C_4H_9)_4[Fe^{II}Fe^{III}(C_2O_4)_3]\}_\infty$ to gain a comprehensive understanding of the process. The thermal decomposition of oxalate-based complexes is usually complicated and proceeds stepwise through a series of intermediate reactions.¹¹ In the present study, two different isoconversional methods, namely, an improved iterative method (to obtain a more accurate value for the activation energy of the reaction)¹² and a model-free method (to obtain reliable and consistent kinetic information from the non-isothermal data)¹³ were employed to analyse the thermogravimetry results, as well as to estimate the kinetic parameters of the thermal decomposition of $\{N(n-C_4H_9)_4[Fe^{II}Fe^{III}(C_2O_4)_3]\}_\infty$. The kinetic parameters of a solid state thermal decomposition reaction have a physical meaning and could be used to study the solid state reaction mechanism *vis-à-vis* the reaction model. Modern kinetics investigation procedure using multi-heating rates for multi-step reactions are also used to determine the correct reaction mechanism function.¹⁴ The variation of the activation energies with the extent of the reactions are discussed to reveal the complexity of the multi-step reactions observed for this material.

EXPERIMENTAL

The precursor material $\{N(n\text{-C}_4\text{H}_9)_4[\text{Fe}^{\text{II}}\text{Fe}^{\text{III}}(\text{C}_2\text{O}_4)_3]\}_{\infty}$, (BuFeFe) was prepared in a one-pot reaction according to a reported procedure.¹⁵ The powdery deep green coloured sample thus obtained was used for the thermogravimetric (TG) study. The measurements were performed using an STA 449C Thermogravimetric analyzer (Netzsch, Germany) under a dry air atmosphere. The sample mass used for TG study was ~ 4 mg. UHP nitrogen (99.999 %) was used as protective gas in the instrument. All the kinetic parameters, namely, the activation energy, the pre-exponential factor, and the reaction model calculations, were performed using a program compiled in MATLAB.

RESULTS AND DISCUSSION

The thermal decomposition of BuFeFe was monitored by TG at three different heating rates (β) 5, 10 and 20 K min⁻¹. The TG curves of BuFeFe obtained at three different heating rates are shown in Fig. 1, from which different thermal decomposition steps can be seen. Thus, a very gradual loss of mass (m) for the three different heating rates commences at around 315 K. The thermal decomposition proceeds with rapid mass loss through three linear steps, indicating different stages of solid state reaction of BuFeFe. These linear steps, which appear in heating rate dependent temperature ranges, are indicated by arrows in Fig. 1, and denoted as Step-I, Step-II and Step-III, respectively, in Table I. It can be seen that the temperature range (ΔT) corresponding to the different steps were shifted

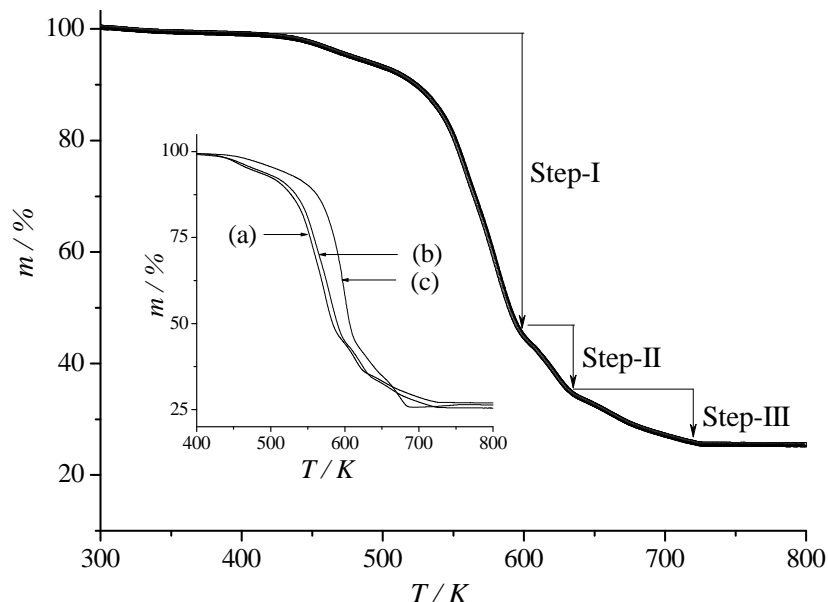


Fig. 1. Thermogravimetric profile of $\{N(n\text{-C}_4\text{H}_9)_4[\text{Fe}^{\text{II}}\text{Fe}^{\text{III}}(\text{C}_2\text{O}_4)_3]\}_{\infty}$ obtained at a heating rate of 10 K min⁻¹. The arrows indicate the different steps of the thermal decomposition. Inset represents the TG profiles of $\{N(n\text{-C}_4\text{H}_9)_4[\text{Fe}^{\text{II}}\text{Fe}^{\text{III}}(\text{C}_2\text{O}_4)_3]\}_{\infty}$ obtained under three different heating rates: a) 5, b) 10 and c) 20 K min⁻¹.

towards higher temperatures with increasing heating rate. For example, in case of Step-I, the loss of mass continues until ≈ 587 K for $\beta = 5$ K min $^{-1}$, until ≈ 598 K for $\beta = 10$ K min $^{-1}$ and until 612 K for $\beta = 20$ K min $^{-1}$. The ΔT and m values corresponding to the different steps under different heating rates, along with the residual mass at 800 K in each case of heating rate are compared in Table I. Step-I corresponds to the largest mass loss in the TG profile. Thus, BuFeFe undergoes successive solid state reactions in three steps. Thermal decomposition becomes complete at ≈ 723 , 718 and 685 K for heating rate 5, 10 and 20 K min $^{-1}$, respectively, with very similar residual masses. It was reported earlier that the decomposition of BuFeFe proceeds through a few intermediate phases and finally results in the formation of a powdery deep red product, which is nothing but the nano-sized ferrite particles (hematite and magnetite).^{9,10}

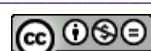
TABLE I. The temperature range of the different steps and the corresponding mass loss values during the thermal decomposition of $\{N(n\text{-C}_4\text{H}_9)_4[\text{Fe}^{\text{II}}\text{Fe}^{\text{III}}(\text{C}_2\text{O}_4)_3]\}_{\infty}$ and associated residual mass values estimated under different heating rates; β = heating rate, ΔT = temperature range, m = loss of mass

β / K min $^{-1}$	Step-I		Step-II		Step-III		Residual mass, %
	ΔT / K	m / %	ΔT / K	m / %	ΔT / K	m / %	
5	315–587	52	587–625	12	625–723	9	27
10	315–598	54	598–633	11	633–718	9	26
20	315–612	54	612–648	11	648–685	10	25

Presently, the thermal decomposition mechanism of BuFeFe is analyzed considering the first two steps of the TG profile only, as it is impractical to consider Step-III. To describe the kinetics of thermal decomposition of BuFeFe reliably, isoconversional methods were used. In the isoconversional method, the reaction rate at constant extent of conversion is assumed to be a function of temperature only.¹⁶ Two simplifying assumptions are used in this regard: *i*) the temperature at any point in the solid remains same and *ii*) the controlling step in the reaction rate does not alter throughout the transformation of a chemical process.¹⁷ Under non-isothermal conditions where the temperature varies linearly with time, *i.e.*, the linear heating rate $\beta = dT/dt = \text{const.}$, the kinetic equation of solid state thermal decomposition is frequently described by the well-known differential rate equation:¹⁸

$$\beta \frac{d\alpha}{dT} = Af(\alpha) \exp\left(-\frac{E^*}{RT}\right) \quad (1)$$

where $\alpha = (m_i - m_t)/(m_i - m_f)$ is the extent of reaction, *i.e.*, the fraction of the material that had reacted in time t , m_i and m_f are the initial and final masses in the particular decomposition step of interest, m_t is the mass at any instant of the reaction in this step, $d\alpha/dT$ is the rate of conversion (in K $^{-1}$), A is the pre-



exponential Arrhenius factor (in min^{-1}), $f(\alpha)$ is the differential conversion function depending on the mechanism of a kinetic reaction,¹⁹ E^* is the activation energy (in kJ mol^{-1}) and R is the universal gas constant (in $\text{kJ mol}^{-1} \text{K}^{-1}$). The variations of the extent of reaction (α) with temperature during the thermal decomposition of BuFeFe during Step-I and Step-II are illustrated in Fig. 2.

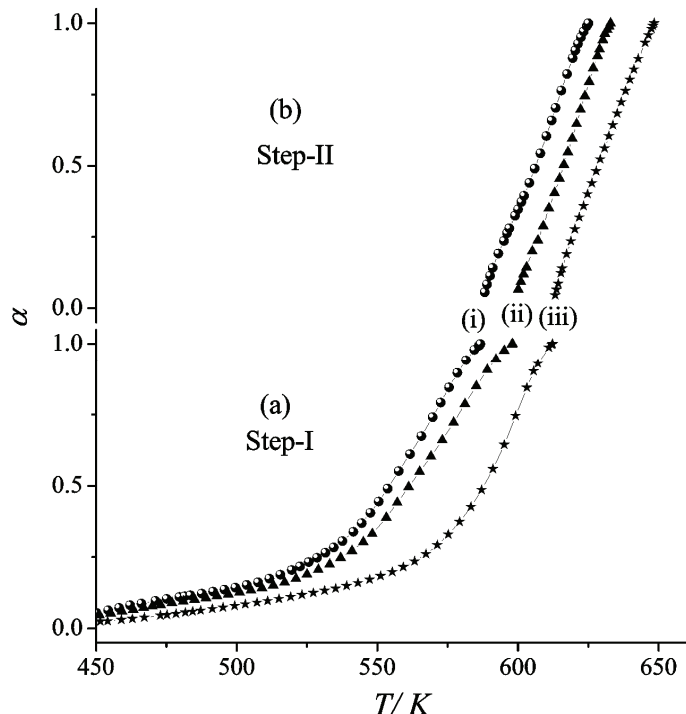


Fig. 2. Variation of the extent of conversion (α) with temperature during the thermal decomposition of $\{N(n\text{-C}_4\text{H}_9)_4[\text{Fe}^{\text{II}}\text{Fe}^{\text{III}}(\text{C}_2\text{O}_4)_3]\}_\infty$ for Step-I (a) and Step-II (b) under different heating rates: i) 5, ii) 10 and iii) 20 K min^{-1} .

The iterative procedure is used to calculate the activation energy, approximating the exact value of activation energy, according to the following equations:¹²

$$\ln \frac{\beta_i}{h(x)T_{\alpha,i}^2} = \ln \frac{A_\alpha R}{g(\alpha)E_\alpha^*} - \frac{E_\alpha^*}{RT_{\alpha,i}} \quad (2)$$

and

$$\ln \frac{\beta_i}{H(x)} = \ln \frac{0.0048 A_\alpha E_\alpha^*}{g(\alpha)R} - 1.0516 \frac{A_\alpha E_\alpha^*}{RT_{\alpha,i}} \quad (3)$$

here $h(x)$ is expressed as:²⁰

$$h(x) = \frac{x^4 + 18x^3 + 88x^2 + 96x}{x^4 + 20x^3 + 120x^2 + 240x + 120} \quad (4)$$

and $H(x)$ is expressed as:¹⁴

$$H(x) = \frac{\exp(-x)h(x)/x^2}{0.0048\exp(-1.0516x)} \quad (5)$$

where $x = E_\alpha^* / RT_{\alpha,i}$. In performing the iterative procedure, the following steps are often used: Step 1 – the initial value of the activation energy $(E_\alpha^*)_1$ is estimated by fitting Eq. (2) or (3) with the assumption $h(x) = 1$ or $H(x) = 1$. Generally, the conventional isoconversional methods stop calculating at this step; Step 2 – using $E_\alpha^* = (E_\alpha^*)_1$, $h(x)$ and $H(x)$ are calculated and a new value of $E_\alpha^* = (E_\alpha^*)_2$ is calculated from the fit of the plot $\ln[\beta_i / h(x)T_{\alpha,i}^2]$ vs. $1/T_{\alpha,i}$ with Eq. (2) or of the plot $\ln[\beta_i / H(x)T_{\alpha,i}^2]$ vs. $1/T_{\alpha,i}$ with Eq. (3); Step 3 – repetition of Step 2 replacing $(E_\alpha^*)_1$ with $(E_\alpha^*)_2$ resulting in $E_\alpha^* = (E_\alpha^*)_3$ and so on until the absolute difference $[(E_\alpha^*)_i - (E_\alpha^*)_{i-1}]$ becomes less than 0.1 kJ mol^{-1} . The last value of $(E_\alpha^*)_i$ thus obtained is considered to be the most accurate estimate of the activation energy (E_α^*) of a thermal reaction. The thus obtained E_α^* values for the present thermogravimetric data, based on Eqs. (2) and (3), are listed in Table II.

In the model-free isoconversional method for non-isothermal thermogravimetry experiments, the activation energy E_α^* can be evaluated at any particular value of α by minimizing the following objective function:^{13,14}

$$\Omega(E_\alpha^*) = \sum_{i=1}^n \sum_{j=1}^n \frac{I(E_\alpha^*, T_{\alpha,i}) \beta_j}{I(E_\alpha^*, T_{\alpha,j}) \beta_i} \quad (6)$$

where $I(E_\alpha^*, T_{\alpha,i})$, the temperature integral, is given as:

$$I(E_\alpha^*, T_{\alpha,i}) = \int_0^{T_{\alpha,i}} \exp\left(-\frac{E_\alpha^*}{RT}\right) dT \quad (7)$$

There are several methods and popular approximations to evaluate this temperature integral. However, the approximation as adopted by Cai *et al.*²¹ is proved to be superior to any of the other approximations and is the most suitable solution for the evaluation of the activation energy, E_α^* , and other kinetic parameters from non-isothermal kinetic analyses. According to this approximation, the temperature integral is given as:²¹

$$\int_0^{T_{\alpha,i}} \exp\left(-\frac{E_\alpha^*}{RT}\right) dT = \frac{RT_{\alpha,i}^2}{E_\alpha^*} \left[\frac{\frac{E_\alpha^*}{RT_{\alpha,i}} + 0.66691}{\frac{E_\alpha^*}{RT_{\alpha,i}} + 2,64943} \right] \exp\left(-\frac{E_\alpha^*}{RT_{\alpha,i}}\right) \quad (8)$$

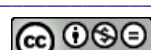


TABLE II. The activation energy, reaction rate and model of reaction mechanism for Step-I and Step-II of the thermal decomposition of $\{N(n\text{-C}_4\text{H}_9)_4[\text{Fe}^{\text{II}}\text{Fe}^{\text{III}}(\text{C}_2\text{O}_4)_3]\}_{\infty}$

Extent of conversion α / min^{-1}	Activation energy, $E_a / \text{kJ mol}^{-1}$						Reaction mechanism	Average value of A / min^{-1}		
	Step-I			Step-II						
	Eq. (2)	Eq. (3)	Eq. (6)	Eq. (2)	Eq. (3)	Eq. (6)				
0.1	58.93	58.93	58.95	155.62	155.62	155.6	Nucleation ^a	4.77×10^4		
0.2	74.07	74.07	74.09	164.65	164.65	164.7	Chemical reaction ^b	5.01×10^{12}		
0.3	82.86	82.86	82.88	174.01	174.01	173.9	reaction ^b	3.87×10^{13}		
0.4	88.47	88.48	88.49	182.29	182.29	182.3		3.14×10^{14}		
0.5	91.04	91.04	91.06	187.25	187.26	187.3		2.67×10^7		
0.6	100.71	100.72	100.7	189.22	189.22	189.2		2.25×10^{15}		
0.7	112.29	112.29	112.3	187.33	187.33	187.3		8.72×10^7		
0.8	125.44	125.44	125.5	183.83	183.83	183.9		4.6×10^7		
0.9	137.69	137.7	137.7	179.72	179.73	179.7		1.98×10^{16}		

^a $g(\alpha) = \ln(\alpha)$, ^b $f(\alpha) = \alpha$; ^a $g(\alpha) = (1-\alpha)^2$, ^b $f(\alpha) = (1-\alpha)^3/2$

$$\int_0^{T_{\alpha,i}} \exp\left(-\frac{E_{\alpha}^*}{RT}\right) dT = \frac{RT_{\alpha,i}^2}{E_{\alpha}^*} \left[\frac{\frac{E_{\alpha}^*}{RT_{\alpha,i}} + 0.66691}{\frac{E_{\alpha}^*}{RT_{\alpha,i}} + 2,64943} \right] \exp\left(-\frac{E_{\alpha}^*}{RT_{\alpha,i}}\right) \quad (8)$$

The minimization procedure was repeated for each value of α from 0.1 to 0.9 for Step-I and Step-II (taking the data from Fig. 2) to determine the dependency of E_{α}^* on α during Step-I and Step-II of the thermogravimetry profile. The E_{α}^* values thus obtained for Step-I and Step-II are presented in Table II. The activation energy (E_{α}^*) values obtained by the three different methods are shown as a function of α in Fig. 3 for Step-I and Step-II. It is noticeable that the E_{α}^* values thus calculated by the three different methods (Eqs. (2), (3) and (6)) are remarkably similar.

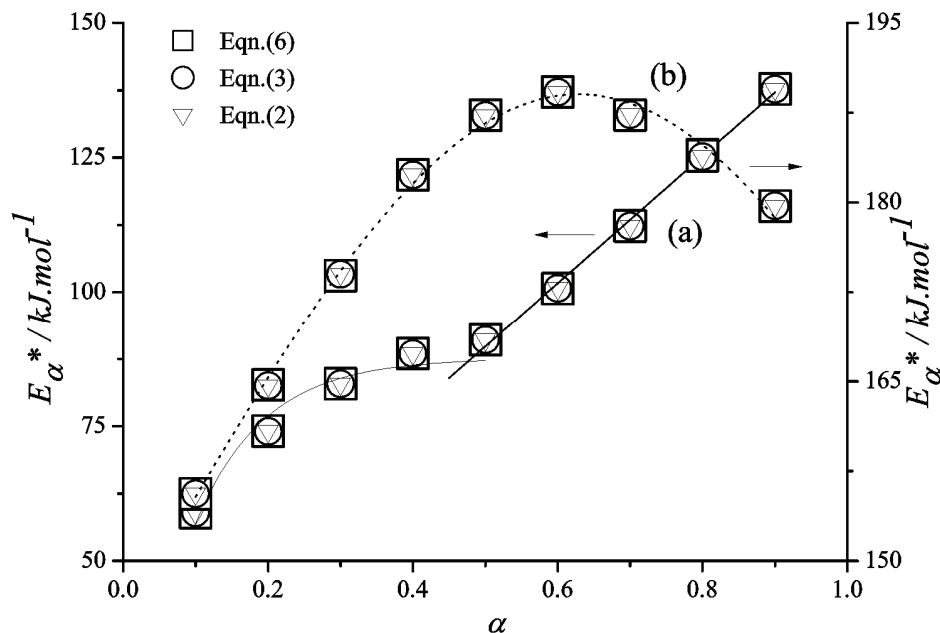


Fig. 3. Dependence of the activation energy on the extent of conversion (α) during the thermal decomposition of $\{N(n-C_4H_9)_4[Fe^{II}Fe^{III}(C_2O_4)_3]\}_\infty$ obtained using different isoconversional methods: a) Step-I and b) Step-II. The arrows indicate the scales used.

From Fig. 3, it is clear that in case of Step-I of the thermal reaction, the E_{α}^* value increased exponentially ($E_{\alpha}^* = a(1-e^{-ba})$, a and b being two fit parameters) for $\alpha \leq 0.4$ and beyond that, E_{α}^* increased linearly with increasing α . Thus, at around $\alpha \approx 0.4$, the rate of reaction became almost saturated. However, the reaction was triggered at $\alpha \approx 0.5$, resulting in the linear E_{α}^* vs. α variation for the

remaining values of α . On the other hand, for Step-II of thermal reaction, the variation of E_α^* vs. α (Fig. 3b) was quite different from that observed for Step-I. Here, the E_α^* value increased with increasing α until $\alpha = 0.6$ and beyond that, the E_α^* value decreased with increasing α . The variation E_α^* with α observed for Step-II could be well-fitted with a Gaussian type distribution function, as shown by the dotted curve in Fig. 3. These different E_α^* vs. α variations, being either intra-step or inter-step thermal decomposition reactions, are the manifestations of different reaction rate control mechanisms involved along these steps.

The integral form of the reaction model describing the reaction mechanism^{16,18} is given by:

$$g(\alpha) = \int_0^\alpha [f(\alpha)]^{-1} d\alpha$$

Some of the frequently used reaction mechanisms operating in solid-state reactions are given in the literature.²² The equation which is mostly used to estimate the correct reaction mechanism, *i.e.*, the $g(\alpha)$ function, is:¹⁴

$$\ln g(\alpha) = \left[\ln \frac{A\alpha E_\alpha^*}{R} + \ln \frac{e^{-x}}{x^2} + \ln h(x) \right] - \ln \beta_i \quad (9)$$

where the symbols have their usual meaning. The values of α corresponding to the multiple heating rates at the same temperature along the α vs. T plots (Fig. 2) were used to generate a plot of $\ln g(\alpha)$ vs. $\ln \beta_i$. For the determination of the correct mechanism function, the slope of the straight line $\ln g(\alpha)$ vs. $\ln \beta_i$, using linear regression, should be equal to -1.0000 and the square of the linear correlation coefficient, R^2 , should be close to unity.¹⁴ While finding the most probable reaction mechanism function $g(\alpha)$ involved in the present thermal decomposition reactions appearing in Step-I and Step-II, 35 types of mechanism functions given in literature²² were used. Incidentally, a number of $g(\alpha)$ functions satisfied the conditions specified above when a particular temperature was used. To remove the confusion, different temperature values were used to arrive at a conclusion about the most probable reaction mechanism function. The most probable reaction mechanism functions, $g(\alpha)$, obtained for the solid state reactions corresponding to Step-I and Step-II of the thermal decomposition profile of BuFeFe according to Eq. (9) are $g(\alpha) = \ln \alpha$ and $g(\alpha) = (1-\alpha)^{-2} - 1$, respectively. Thus, Step-I of the TG profile corresponds to "nucleation" as the rate-controlling mechanism, whereas Step-II of the profile corresponds to "chemical reaction".²²

Using the estimated value of the activation energy and the most probable reaction model, the value of the pre-exponential or frequency factor (A) can be evaluated from the following equation.^{23,24}



$$A = -\frac{\beta_{x_p}}{Tf'(\alpha_p)} \exp(x_p) \quad (10)$$

where $x_p = E_\alpha^* / RT_p$ (T_p is the peak temperature on the corresponding differential thermogravimetric curve), $f'(\alpha_p)$ is the first derivative of the kinetic model function. The A values are thus determined for Step-I and Step-II of the TG profile of BuFeFe for different values of α under different heating rates. The variations of A with α under different heating rates are shown in Fig. 4. The effect of heating rate on the A values was found not to be remarkable. However, the dependence of A on the α values were quite noticeable and were different for Step-I and Step-II. For Step-I, the variation of $A(\alpha)$ was similar to that observed for the variation of E_α^* but for Step-II, the values of $A(\alpha)$ increased linearly up to $\alpha \approx 0.5$ and then become nearly independent of α , in contrast to the corresponding $E_\alpha^*(\alpha)$ variation in the same temperature region. The average values of A estimated for the different heating rates are presented in Table II as a function of

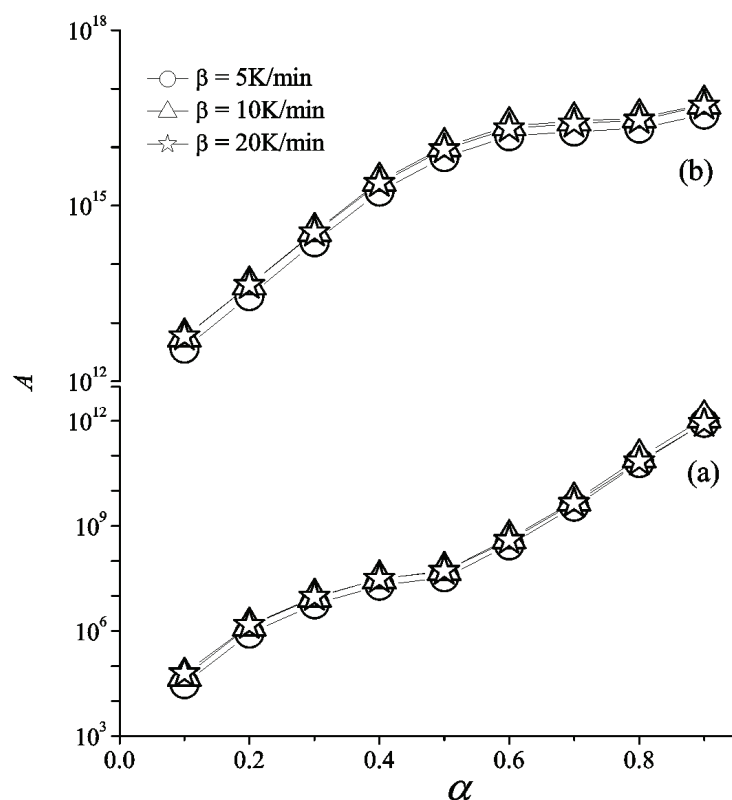
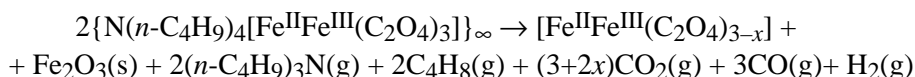


Fig. 4. Dependence of the frequency factor (A / min^{-1}) on the extent of conversion (α) during the thermal decomposition of $\{N(n\text{-C}_4\text{H}_9)_4[\text{Fe}^{II}\text{Fe}^{III}(\text{C}_2\text{O}_4)_3]\}_\infty$: a) Step-I and b) Step-II.

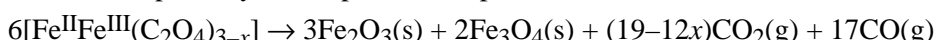
the α values. The rate of reaction for the decomposition of BuFeFe varied in the range of 10^3 – 10^{12} min $^{-1}$ and 10^{12} – 10^{18} min $^{-1}$ for Step-I and Step-II, respectively. Thus, for both steps of the reaction, the A values varied by an order of 10^9 and 10^6 for Step-I and Step-II, respectively. This indicates that the reaction rate cannot be assumed to be a constant for the studied non-isothermal decomposition process. Interestingly, from Table II, it could be seen that the greatest number of A values were grouped about the order of 10^{15} min $^{-1}$ in Step-II within a narrow E_a^* range, while for Step-I, the A values were distributed over a wide range of E_a^* values. The values of A in solid state reactions are expected to be in a wide range.²² Low factors often indicate a surface reaction. If the reactions are not dependent on the surface area, a low A value indicates a “tight” complex, while a higher A value indicates a “loose” complex. Accordingly, in the present case, Step-I may involve loose and tight complexes, whereas Step-II involves a tight complex only.

Considering the mass loss values during the different thermal decompositions of BuFeFe, observed in the thermogravimetry profile, the reaction pathway(s) as well as the reaction product(s) at the end of the successive reaction step(s) of the thermal decomposition have already been reported by the authors.⁹ The thermal decomposition process of BuFeFe was proposed as follows:

Reaction pathway for Step-I:

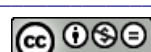


Reaction pathway for Step-II and Step-III:



where g and s denote gaseous and solid substances, respectively and x is a positive number (< 3). The observed mass loss values compare well with the calculated mass loss values following the proposed reaction pathways. Thus, the proposed reaction pathways indicate the formation of either Fe_3O_4 (magnetite) or Fe_2O_3 (hematite) or a mixture of both as the end-product of the thermal decomposition of the molecular magnetic precursor BuFeFe. The formation of the proposed end products was supplemented by IR and powder XRD studies and confirmed by magnetic studies.⁹ Incidentally, at present the authors have studied the reaction kinetics of Step-I and Step-II. An attempt to continue the calculation of kinetic parameters to Step-III was avoided because of practical difficulties as Step-III corresponds to very small mass loss, which, if considered, would have introduced an erroneous result due to the large error associated with the $\alpha(T)$ values.

Along the above-stated step-wise reaction pathways, during Step-I of the thermal decomposition, the bimetallic 3-dimensional network structure of $\{N(n-C_4H_9)_4[Fe^{II}Fe^{III}(C_2O_4)_3]\}_\infty$ is disrupted completely. Here the organic cationic



part, $N(n\text{-C}_4\text{H}_9)_4^+$, decomposes giving rise to various gaseous substances, while the 2-dimensional $\text{Fe}^{\text{III}}\text{-oxalate}\text{-}\text{Fe}^{\text{II}}$ anionic layers are partially degraded giving rise to Fe_2O_3 . It is apparent that the former process may require a lower activation energy than the latter and will be completed faster due to the limited abundance. The partial decomposition of the $\text{Fe}^{\text{III}}\text{-oxalate}\text{-}\text{Fe}^{\text{II}}$ anionic layers may be due to scission of the metal–oxalate linkages. In this way, the initial exponential growth in the $E_{\alpha}^* \text{ vs. } \alpha$ plot for Step-I may be due to the decomposition of $N(n\text{-C}_4\text{H}_9)_4^+$, while the steady linear $E_{\alpha}^* \text{ vs. } \alpha$ variation in the later part of Step-I may be due to decomposition of the bimetallic network and formation of metal oxides. The reaction mechanism responsible for this step of the thermal decomposition was resolved to be nucleation given by $g(\alpha) = \ln \alpha$, an acceleratory rate equation.²²

The early stage of Step-II supposedly favours the gradual decomposition of the bimetallic network and formation of metal oxides, giving rise to a steady growth in the $E_{\alpha}^* \text{ vs. } \alpha$ variation. It should be noted that the activation energy required for the linear part of the $E_{\alpha}^* \text{ vs. } \alpha$ plot in Step-I and those for the initial growth part of the $E_{\alpha}^* \text{ vs. } \alpha$ plot in Step-II lie in the same range. The Gaussian type variation of E_{α}^* with α is certainly the manifestation of a reaction control mechanism owing to the residual amount of reactants, *i.e.*, the remaining amount of thermally degradable molecules as well as the *in situ* degraded gaseous products. It should be noted that the thermal decomposition of iron oxalate to hematite in an air atmosphere and to magnetite in presence of CO/CO_2 mixture was reported by other workers.²⁵ The thermal decomposition initially started in air atmosphere leading to the formation of hematite along with a profuse amount of CO_2 and subsequently, on further heating, it might have led to the formation of magnetite.²⁶ The reaction mechanism responsible for Step-II of thermal decomposition observed in the present study was resolved to be a chemical reaction type.²²

CONCLUSIONS

The present study demonstrates the kinetics of solid state reaction of the thermal decomposition of $\{N(n\text{-C}_4\text{H}_9)_4[\text{Fe}^{\text{II}}\text{Fe}^{\text{III}}(\text{C}_2\text{O}_4)_3]\}_{\infty}$ at multiple heating rates. The thermal decomposition proceeds through three different steps, indicating three reaction mechanisms. The reaction mechanism responsible for Step-I of the thermal decomposition was resolved to be nucleation whereas Step-II is of a chemical reaction type. Calculation of kinetic parameters for Step-III was avoided due to practical difficulties. Step-wise reaction pathways leading to ferrites were proposed. The rates of the reactions were in the range of $10^3\text{--}10^{12}$ and $10^{12}\text{--}10^{18} \text{ min}^{-1}$ for Step-I and Step-II, respectively.

It would be of interest to know the nature of the dependence of the reaction kinetics and the reaction mechanism on the sample environment. The identi-

fication of the various reaction products at the end of each step of the TG profile is necessary and thereby the complete reaction pathway. These studies require an *in situ* FT-IR study and evolved gas analysis (EGA), which subjects of our present interest. These results would provide insight into the mechanism of external control of the solid state thermal reactions in order to yield interesting ferrite materials using molecular complex precursors through the thermal decomposition route.

ИЗВОД

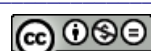
ТЕРМАЛНА ДЕКОМПОЗИЦИЈА МОЛЕКУЛАРНОГ МАТЕРИЈАЛА
 $\{N(N\text{-C}_4\text{H}_9)_4[\text{Fe}^{\text{II}}\text{Fe}^{\text{III}}(\text{C}_2\text{O}_4)_3]\}_{\infty}$ ДО ФЕРИТА: ИСПИТИВАЊЕ РЕАКЦИОНЕ КИНЕТИКЕASHIS BHATTACHARJEE¹, DEBASIS ROY¹, MADHUSUDAN ROY² и ARUNABHA ADHIKARI³¹*Department of Physics, Visva-Bharati University, Santiniketan, India*, ²*Applied Material Science Division, Saha Institute of Nuclear Physics, Kolkata, India* и ³*Department of Physics, West Bengal State University, Barasat, India*

Термална декомпозиција молекуларног прекурсора, $\{N(n\text{-C}_4\text{H}_9)_4[\text{Fe}^{\text{II}}\text{Fe}^{\text{III}}(\text{C}_2\text{O}_4)_3]\}_{\infty}$ која се одвија у више ступњева, испитивана је неизотермским термогравиметријским (ТГ) мерењима у температурском опсегу од 300 до ≈ 800 К при различитим брзинама грејања (5, 10 и 20 K min⁻¹). Термална декомпозиција комплекса на бази оксалата се одвија ступњевито кроз низ реакција. Коришћењем две различите изоконверзионе методе, тачније, унапређене итеративне методе и методе без модела одређени су кинетички параметри: енергија активације и брзина реакције, и највероватнији реакциони механизам термалне декомпозиције. Различити реакциони путеви који резултују у различитим ступњевима термогравиметријских профиле су такође разматрани коришћењем ранијих експерименталних резултата истих аутора.

(Примљено 19. маја 2012)

REFERENCES

1. M. Winter, R. J. Brodd, *Chem. Rev.* **104** (2004) 4245
2. M. M. Thackeray, C. S. Johnson, J. T. Vaughey, N. Li, S. A. Hackney, *J. Mater. Chem.* **15** (2005) 2257
3. G. Eranna, B. C. Joshi, D. P. Runthala, R. P. Gupta, *Crit. Rev. Solid State Mater. Sci.* **29** (2004) 111
4. M. E. Franke, T. J. Koplin, U. Simon, *Small* **2** (2006) 36
5. K. L. Chopra, P. D. Paulson, V. Dutta, *Prog. Photovoltaics* **12** (2004) 69
6. M. L. Kahn, A. Glaria, C. Pages, M. Monge, L. Saint Macary, A. Maisonnat, B. Chaudret, *J. Mater. Chem.* **19** (2009) 4044
7. A. Bhattacharjee, S. Reiman, V. Ksenofontov, P. Gütlich, *J. Phys. Condens. Matter.* **15** (2003) 5103
8. K. E. Neo, Y. Y. Ong, H. V. Huynh, T. S. Andy Hor, *J. Mater. Chem.* **17** (2007) 1002
9. A. Bhattacharjee, D. Roy, M. Roy, *J. Therm. Anal. Calorim.* **109** (2012) 1423
10. A. Bhattacharjee, D. Roy, M. Roy, S. Chakraborty, A. De, J. Kusz, W. Hofmeister, *J. Alloy. Compd.* **503** (2010) 449
11. F. A. Cotton, G. Wilkinson, C. A. Murillo, M. Bochmann, *Advanced Inorganic Chemistry*, 6th ed., Wiley, New York, 1999



12. Z. Gao, M. Nakada, I. Amasaki, *Theromochim. Acta* **369** (2001) 137
13. S. Vyazovkin, D. Dollimore, *J. Chem. Inf. Comput. Sci.* **36** (1996) 42
14. L. Liqing, C. Donghua, *J. Therm. Anal. Calorim.* **78** (2004) 283
15. H. Ōkawa, N. Matsumoto, H. Tamaki, S. Kida, M. Ohba, *Mol. Cryst. Liq. Cryst.* **233** (1993) 257
16. S. Vyazovkin, in *The Handbook of Thermal Analysis & Calorimetry, Vol. 5: Recent Advances, Techniques and Applications*, M. E. Brown, P. K. Gallagher, Eds., Elsevier, Amsterdam, The Netherlands, 2008, p. 503
17. A. W. Coats, J. P. Redfern, *Nature* **201** (1964) 68
18. J. Farjas, P. Roura, *J. Therm. Anal. Calorim.* **105** (2011) 767
19. J. Šesták, *Thermophysical Properties of Solids, Their Measurements and Theoretical Analysis*, Vol. 12D, Elsevier, Amsterdam, The Netherlands, 1984
20. G. I. Senum, R. T. Yang, *J. Therm. Anal. Calorim.* **11** (1977) 445
21. J. Cai, F. Yao, W. Yi, F. He, *AIChE J.* **52** (2006) 1554
22. L. Vlaev, N. Nedelchev, K. Gyurova, M. Zagorcheva, *J. Anal. Appl. Pyrolysis* **81** (2008) 253
23. J. Málek, *Thermochim. Acta* **200** (1992) 257
24. B. Janković, S. Mentus, M. Janković, *J. Phys. Chem. Solids* **69** (2008) 1923
25. A. Angermann, J. Töffer, *J. Mater. Sci.* **43** (2008) 5123
26. I. S. Lyubutin, C. R. Lin, Yu. V. Korzhetskiy, T. V. Dmitrieva, R. K. Chiang, *J. Appl. Phys.* **106** (2009) 34311.

